7th IAA Planetary Defense Conference – PDC 2021
26–30 April 2021, Vienna, Austria

IAA-PDC21-0X-YY

Effect of non-Keplerian MOID evolution on preliminary keyhole analyses

Oscar Fuentes-Munoz[a,1,*], Anivid Pedros-Faura[a,1], Davide Amato[a,b,2,3]

[a] *Colorado Center for Astrodynamics Research, University of Colorado Boulder, 429 UCB, 3775 Discovery Drive, Boulder, Colorado, 80303, United States*
[b] *Department of Aeronautics, Imperial College London, South Kensington Campus, London, SW7 2AZ, United Kingdom*

Abstract

During close encounters asteroids can cross keyholes, regions in the vicinity of a planet that lead to a future collision. The location of keyholes in resonant encounters can be computed analytically on the B-plane[1]. If an asteroid crosses a keyhole, the close encounter geometry will repeat itself after the corresponding integer amount of years.

The analytical computation of the location of keyholes in the B-plane assumes that the asteroid undergoes Keplerian motion between encounters. As a consequence, the minimum orbit intersection distance (MOID) remains constant. During the preliminary analysis of the collision probability this is a very useful approximation. Nonetheless, the heliocentric orbit between encounters is perturbed by other bodies of the solar system.

In this paper we investigate the effect of a perturbed MOID on the keyholes of 2021 PDC.We consider three approaches with increasing levels of refinement for the calculation of the keyholes of 2021 PDC. The first consists in assuming that the MOID is constant across encounters. In the second, we compute the MOID from a semi-analytical propagation, accounting for the influence of Jupiter only. In the third, we compute the MOID from a numerical propagation, accounting for the gravitational perturbations from all planets. We analyze the impact that the MOID evolution has on the actual keyhole map on the B-plane comparing the three approaches. Based on our results, we also analyze how short-period effects can modify the MOID and how Earth's eccentricity plays an important role in our mapping.

Keywords: Near-Earth Asteroid, Astrodynamics, MOID, Keyhole, Close Encounters

1. Introduction

The risk of collision with Earth of Near Earth Asteroids (NEAs) is of great interest from a planetary defense perspective. Close encounters abruptly change the orbits of NEAs potentially posing a hazard for life on Earth in the future. For this reason the work presented aims to provide tools to better characterize the collision probability of hazardous objects.

Planetary encounters introduce nonlinearities and chaos in the motion of solar system bodies[1]. For this reason, modelling the post-encounter trajectory is key to assess the future risk of collision. Once a close encounter with Earth happens, computing the **keyholes** becomes important to predict future collision risk. From this first encounter of the asteroid with the planet, we can define a *keyhole* as each subsequent return that could lead to an impact on the target plane of the first encounter[2].

*Corresponding author
Email addresses: Oscar.FuentesMunoz@colorado.edu (Oscar Fuentes-Munoz), Anivid.PedrosFaura@colorado.edu (Anivid Pedros-Faura), d.amato@imperial.ac.uk (Davide Amato)
[1] Graduate Research Assistant, University of Colorado Boulder.
[2] Postdoctoral Associate, University of Colorado Boulder.
[3] Lecturer, Imperial College London.

Previous work exists to determine the location of keyholes on the B-plane [2][3][4]. However, it is assumed that the asteroid undergoes Keplerian motion between encounters with the planet of study. This assumption can become an important limitation in the frequent case that other bodies perturb the asteroid. The location of keyholes must be taken into account in asteroid deflection studies[4]. Our goal in this paper is to improve the computation of keyholes by using more realistic dynamics for the trajectory propagation of the asteroid and apply it to the 2021 PDC asteroid case. In the B-plane and assuming the orbit of the planet circular, the ξ coordinate corresponds to the minimum orbit intersection distance (MOID). In this paper we will analyze the effects of non-Keplerian dynamics of the MOID between encounters to find the modified location of keyholes or modified keyholes.

Our work is presented as follows. A brief introduction on how to model close encounters is provided in section 2, along with useful tools and definitions. In section 3 the MOID algorithm and dynamics models used are presented. With this theoretical background, the keyhole computation criterion is finally presented in section 4 for both Keplerian and non-Keplerian motion assumptions. Numerical results are provided for each method, assuming the Earth's orbit to be circular. Lastly, a more realistic case with an eccentric Earth's orbit is discussed following the same techniques (Section 5). Throughout the paper the flyby of 2021 PDC is used as benchmark for the developed theory of modified keyholes.

2. Close encounters and the B-plane

Planetary encounters cause the orbits of near-Earth objects to abruptly change in time scales of days. The change in the heliocentric elements is very sensitive to initial conditions of the flyby. This section defines in detail the process of extraction of ephemeris, frame transformations and evaluation of the encounter used in the present work. The heliocentric coordinates of the NEO are mapped to the B-plane, a planetocentric reference frame to used analyze the encounter. The modified target plane (MTP) allows to uniquely define the flyby, hence it is used to define the encounter coordinates. Then, the encounter is solved and the new set of heliocentric elements are obtained.

2.1. The B-plane

First, we obtain the heliocentric Cartesian coordinates of asteroid and planet when the asteroid is in the vicinity of the planet. Then, the heliocentric coordinates are mapped to a planetocentric frame defined as: center at the planet, Y-axis aligned with the direction of the planet motion, the Z-axis parallel to the angular momentum vector of the planet, and X-axis completing the frame. The B-plane orientation is normal to the relative asymptotic velocity U in the planetocentric frame [5]. Using the vector components of U we obtain the angles θ, ϕ:

$$\begin{bmatrix} U_x \\ U_y \\ U_z \end{bmatrix} = \begin{bmatrix} U \sin\theta \sin\phi \\ U \cos\theta \\ U \sin\theta \cos\phi \end{bmatrix} \tag{1}$$

The angles θ, ϕ are used to map the relative position to the B-plane coordinates ξ–η–ζ as the consecutive following rotations: a rotation of $-\phi$ about Y and a rotation of $-\theta$ about ξ -positive counterclockwise-. This rotation can be applied at any time during the planetary flyby. As explained in the following section, in this work we apply this rotation at the time of periapses of the flyby, leading to equation 3.

2.2. The Modified Target Plane

The ephemeris date used to obtain the B-plane coordinates is a free parameter. Using the modified target plane (MTP) this time is defined uniquely as the time of periapsis t_p.[6] The MTP coordinates are mapped to the B-plane using 2-body planetocentric relations from conservation of energy and angular momentum. These B-plane coordinates are used to solve the encounter. Figure 1 shows the two reference planes and the relations between the coordinates in both are found below.

The process to obtain these elements is as follows: we convert the relative Cartesian coordinates to planetocentric Keplerian elements, and obtain the time of perapsis t_p. Then, we generate the set the planetocentric coordinates at the time of periapsis. We denote variables at periapses with the subindex p. Using the relative velocity at periapsis $\boldsymbol{v_p}$ we obtain the angles θ_p, ϕ_p from equation 1:

$$\begin{bmatrix} \cos\theta_p \\ \tan\phi_p \end{bmatrix} = \begin{bmatrix} v_{p,y}/v_p \\ v_{p,x}/v_{p,z} \end{bmatrix} \tag{2}$$

Using these angles we obtain the position in the modified target plane (ξ_p, ζ_p) from the planetocentric coordinates $\boldsymbol{r_p} = (\boldsymbol{X_p}, \boldsymbol{Y_p}, \boldsymbol{Z_p})^T$:

$$\begin{bmatrix} \xi_p \\ \eta_p \\ \zeta_p \end{bmatrix} = \hat{\boldsymbol{R}}_{\xi_p}(-\theta_p)\hat{\boldsymbol{R}}_{Y_p}(-\phi_p)\begin{bmatrix} X_p \\ Y_p \\ Z_p \end{bmatrix} \tag{3}$$

From these coordinates we obtain the B-plane coordinates using energy and angular momentum conservation:

$$U^2 = 2\frac{GM_p}{r_p} + v_p^2 \tag{4}$$

$$r_p v_p = bU \tag{5}$$

$$\begin{aligned} \zeta &= \left(\tfrac{v_p}{U}\right)\zeta_p \\ \xi &= \left(\tfrac{v_p}{U}\right)\xi_p \end{aligned} \tag{6}$$

The relative velocity at perigee is rotated counter-clockwise by an angle $\gamma/2$ about the angular momentum vector of the hyperbola, where γ corresponds to the deflection angle. It is defined as a function of the relative velocity U, and the mass of the planet in units of the Sun m.

$$\tan\frac{\gamma}{2} = \frac{m}{bU^2} = \frac{c}{b} \tag{7}$$

where $c = m/U^2$. The rotated relative velocity defines the orientation of the B-plane θ, ϕ. These B-plane coordinates are used to solve the close encounter as defined in the following section.

$$\boldsymbol{U} = U\hat{\boldsymbol{R}}_h\left(-\frac{\gamma}{2}\right)\hat{\boldsymbol{v}}_{\boldsymbol{p}} \tag{8}$$

2.3. Encounter solution

In Fig.1 the target and modified target plane are presented together with the relative velocities of the flyby.

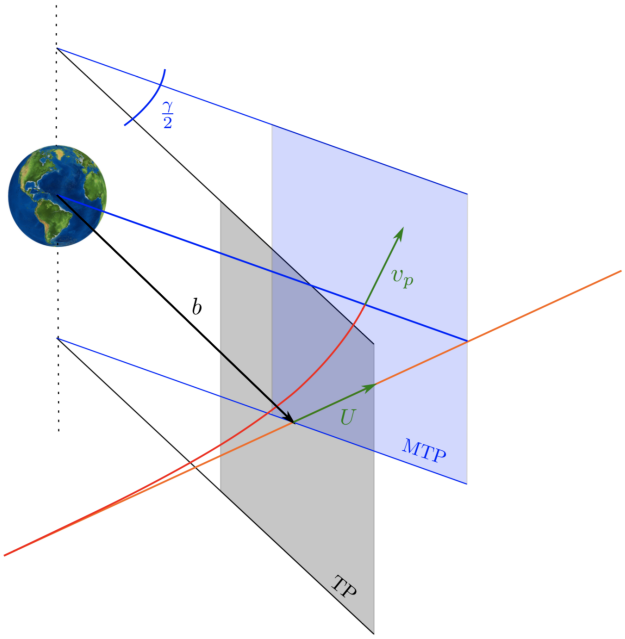

Figure 1: Planetary flyby target planes. The modified target plane (MTP) is defined at periapsis and the target plane (TP) by the asymptotic velocity, as related by equation 7.

The effect of the planetary encounter is a rotation of the relative velocity by a deflection angle γ. The B-plane rotates with the relative velocity, thus the post-encounter B-plane coordinates are found accordingly.

$$\boldsymbol{U}' = \hat{\boldsymbol{R}}_h(\gamma)\boldsymbol{U} \tag{9}$$

$$\boldsymbol{b}' = \hat{\boldsymbol{R}}_h(\gamma)\boldsymbol{b} \tag{10}$$

These equations can be rewritten into scalar components for each of the post-encounter coordinates[2]. The post-encounter heliocentric elements are obtained from the direct mapping of B-plane coordinates to Keplerian elements as reported in [3].

2.4. Resonant returns

The condition for a resonant encounter is that the post-encounter semi-major axis a' presents a commensurability between the orbital periods of the planet and the asteroid. In that situation, after k planet periods and h asteroid periods, a resonant encounter occurs. The condition on the semi-major axis becomes:

$$a_R'^{\,3} = a_p^3 \frac{k^2}{h^2} \tag{11}$$

The locus of points in the B-plane that fulfill the condition of a resonant semi-major axis a' is a resonant circle of radius R centered in $(0, D)$ with parameters R, D[2]:

$$R = \left| \frac{c \sin\theta_R'}{\cos\theta_R' - \cos\theta} \right| \tag{12}$$

$$D = \frac{c \sin\theta}{\cos\theta_R' - \cos\theta} \tag{13}$$

where

$$\cos\theta_R' = \frac{1 - U^2 - 1/a_R'}{2U} \tag{14}$$

If unperturbed Keplerian motion is assumed between encounters, no change in geometry happens for the next encounter. Therefore, we can state:

$$U'' = U' = U, \quad \theta'' = \theta', \quad \phi'' = \phi' \tag{15}$$

Assuming the planet is in a circular orbit, the B-plane coordinate ξ is the MOID between the asteroid and the planet. Based on the previous assumptions, ξ remains constant between encounters, thus:

$$\xi'' = \xi' \tag{16}$$

and the timing component of the flyby ζ'' becomes:

$$\zeta'' = \zeta' - [mod(h \cdot 2\pi a'^{3/2} + \pi, 2\pi) - \pi] \sin\theta' \tag{17}$$

In order to study the Earth flyby of 2021 PDC we use its ephemeris file and the planetary ephemeris DE431[7]. The resonant circles of the 2021 PDC flyby are shown in figure 2.

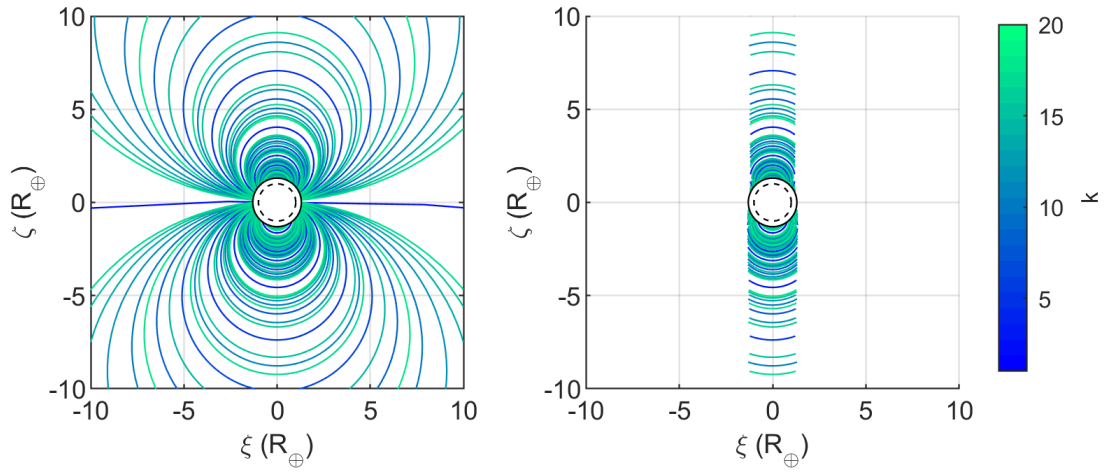

Figure 2: Resonant circles (left) and keyholes (right) of the Earth flyby of 2021 PDC for up to $k = 20$ Earth revolutions. The white circle represents the Earth radius with its gravitational focusing factor and the physical radius (dashed).

3. MOID propagation

3.1. MOID Definition and Computation

The Minimum Orbit Intersection Distance (MOID) is a measure used in astronomy to assess potential close approaches and collision risks between astronomical objects[8], defined as the minimum of the distances between all points belonging to the osculating orbits of two bodies.

A requirement for an impact trajectory is that the MOID between the asteroid and the planet is smaller than the collision radius, which is usually the radius of the planet with the gravitational focusing correction factor.

To compute the MOID, the algorithm proposed by Wisnioski and Rickman [8] is used. The choice has been made based on its performance, accuracy, and flexibility.

3.2. MOID propagation by Secular Model

The orbits of asteroids in the inner solar system are perturbed by planets. The inner solar system planets perturb the orbits of asteroids in flybys and in orbital resonances around specific values of semi-major axis. For asteroids in the vicinity of Earth, Jupiter is the main perturber over long time scales. An analytical solution of this perturbation is derived from the secular terms of the perturbing potential. This assumption ignores short-period components that can play a significant role in the years between resonant encounters, a concern that is addressed in the following sections.

The secular propagation of the MOID is obtained as a result of the secular propagation of the orbit of the asteroid. The secular perturbation is obtained from the integration of Lagrange Planetary Equations with an averaged perturbing potential. In this work we analyze Jupiter as the only perturber of the orbit of 2021 PDC, an common assumption in the inner solar system. Noting with the subindex J the variables referencing Jupiter, the perturbing potential is:

$$R_J = GM_J \left(\frac{1}{|\boldsymbol{r} - \boldsymbol{r}_J|} - \frac{\boldsymbol{r} \cdot \boldsymbol{r}_J}{|\boldsymbol{r} - \boldsymbol{r}_J|} \right) \tag{18}$$

Then we apply the averaging principle to the perturbing potential to retain only secular components. Assuming that eccentricities and inclinations of both perturber planet and asteroid are small, the expansion retains only a few terms and the solution is analytical. The solution of the secular perturbation of a system of small eccentricities and inclinations is known as the Laplace-Lagrange solution[9], suitable for the long-term dynamics of the planets of the solar system.

The secular long-term dynamics of asteroids can be studied as the Laplace-Lagrange solution of the planets perturbing a massless particle. The assumptions on eccentricity and inclination limit the applicability of the secular model to a fraction of the population of NEOs. However, other secular models could be used such as the Lidov-Kozai cycle, in which eccentricity and/or inclination are large. Other non-singular sets of elements such as mean Milankovitch could be used.

We apply this model to compute the jovian perturbation of asteroids in the inner solar system. The orbit of Jupiter is assumed to be external at all times, that is, $|r_J| > |r|$ at all times. We can rewrite the perturbing potential in terms of the Keplerian elements of the asteroid and Jupiter. The new potential is function of the ratio between semi-major axis $\alpha_J = a/a_J$:

$$R_J = C_0 + C_1 \left[\frac{e^2}{2} - \frac{i^2}{2} - \kappa e e_J \cos(\varpi - \varpi_J) + i i_J \cos(\Omega - \Omega_J) \right] \tag{19}$$

where the constants are:

$$C_0 = \frac{GM_J}{2a_J} b^{(0)}_{1/2}(\alpha_J) \tag{20}$$

$$C_1 = n^2 a^2 \frac{1}{4} \frac{M_J}{M + M_{ast}} \alpha_J^2 b^{(1)}_{3/2}(\alpha_J) \tag{21}$$

$$\kappa = \frac{b^{(2)}_{3/2}}{b^{(1)}_{3/2}} \tag{22}$$

These depend on the Laplace Coefficients $b^{(j)}_s(\alpha)$, that are defined as:

$$\frac{1}{2} b^{(k)}_s(\alpha) = \frac{1}{2\pi} \int_0^{2\pi} \frac{\cos(k\psi) d\psi}{(1 - 2\alpha\cos\psi + \alpha^2)^s} \tag{23}$$

Next we convert the perturbing potential to semi-equinoctial elements:

$$\begin{aligned} h &= e \sin\varpi & p &= I \sin\Omega \\ k &= e \cos\varpi & q &= I \sin\Omega \end{aligned} \tag{24}$$

Including the two remaining elements $L = \sqrt{GMa}$ and the mean anomaly at epoch σ, the equations of motion are obtained from the Lagrange Planetary Equations:

$$\begin{aligned} \dot{p} &= \frac{1}{na^2} \frac{\partial R_J}{\partial q} & \dot{h} &= \frac{1}{na^2} \frac{\partial R_J}{\partial k} & \dot{L} &= \frac{\partial R_J}{\partial \sigma} \\ \dot{q} &= -\frac{1}{na^2} \frac{\partial R_J}{\partial p} & \dot{k} &= -\frac{1}{na^2} \frac{\partial R_J}{\partial h} & \dot{\sigma} &= -\frac{\partial R_J}{\partial L} \end{aligned} \tag{25}$$

The solution for the perturbing potential R_j in equation 21 is the oscillation of the elements and a continuous drift in σ:

$$\begin{aligned} h(t) &= S \sin(gt + \beta) + \kappa h_J & p(t) &= T \sin(-gt + \gamma) + p_J \\ k(t) &= S \cos(gt + \beta) + \kappa k_J & q(t) &= T \cos(-gt + \gamma) + q_J \end{aligned} \tag{26}$$

$$\sigma(t) = \sigma_0 + \dot{\sigma} t \tag{27}$$

where $g = -C_1/na^2$ are the oscillation frequencies, and S, T, β, γ are integration constants specified by the initial conditions. This solutions allows the analytical propagation of the heliocentric orbit of asteroids under the perturbation of Jupiter. In order to compute the MOID at a future time, we compute the orbit at the desired time and use the regular MOID algorithm.

3.3. MOID propagation by Numerical integration of n-3BP

In this approach, we propagate the heliocentric orbit of the asteroid numerically under the influence of gravitational perturbations from all planets. We have accounted all the planets of the solar system and worked under the assumption that they follow Keplerian orbits. This choice was made so that we can maintain the encounters as well as capture long and short-term perturbations effects over time.

The perturbing force contribution to the equations of motion for n_p bodies is:

$$\boldsymbol{f}_{3B} = \sum_{j=3}^{n_p} GM_j \left(\frac{\boldsymbol{r}_{2j}}{r^3_{2j}} - \frac{\boldsymbol{r}_{1j}}{r^3_{1j}} \right) \tag{28}$$

where the subscript j represents each specific body. In this case: $j = 1$ refers to the central body -Sun- and $j = 2$ the asteroid. Thus, $\boldsymbol{r}_{1j}$ is the position vector of M_j body with respect to the Sun and

$\boldsymbol{r}_{2j}$ with respect to the asteroid. The elements of the planets are constant and extracted from planetary ephemeris[7] at the same date that the asteroid ephemeris was retrieved.

These equations have been integrated using MATLAB's *ode113* function. *ode113* is a variable-step, variable-order (VSVO) Adams-Bashforth-Moulton PECE solver of orders 1 to 13. The highest order used appears to be 12, and the 13th order is used for the error estimate [10].

3.4. Perturbed propagation of the trajectory and the MOID

The virtual asteroids are propagated from the post-encounter elements using the three models described above. In all cases we find a resonant encounter that occurs after the corresponding h asteroid periods. As an example of this propagation, we show a virtual 2021 PDC that crosses the keyhole in the resonant circle $\{k = 7, h = 5\}$ assuming the Earth is in a circular-ecliptic orbit. The initial conditions are detailed in table 1. In Figure 3 we show the distance d between the asteroid and the Earth time recorded with the three approaches used: Keplerian propagation, secular model, and n-3BP model. This is the actual distance between the asteroid and the Earth recorded over time. The differences in the distance at the subsequent time of closest approach between the three models are of the order of the collision radius, defined as the Earth's radius multiplied by the gravitational focusing factor. Thus, these differences drive the definition of the initial point in the resonant circle as keyhole.

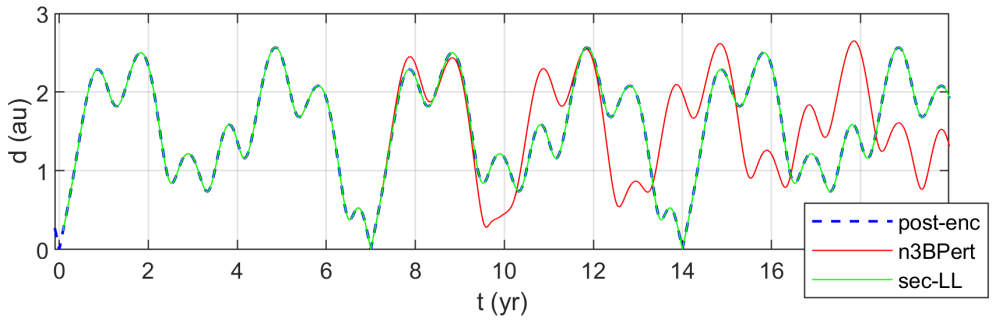

Figure 3: Distance between Earth and the fictitious 2021 PDC that crosses the resonant circle $\{k = 7, h = 5\}$ using three models: constant set of heliocentric elements (blue), secularly perturbed by Jupiter using the Lagrange-Laplace solution (green) and by numerical integration with the 8 planets as perturbers (red). Time is measured in Earth periods from the 2021 encounter epoch with initial conditions as in table 1.

The propagation of the MOID is shown for the same virtual 2021 PDC in figure 4 using the initial conditions in table 1. Here we note the influence of the short-period perturbations in the orbit of the asteroid. In only a few orbits after the initial encounter these oscillations can be of the order of the collision radius. This is the case of the orbit of 2021 PDC. However, in other asteroids these are found to be a minor contribution to the secular which better characterizes the dynamics after the initial encounter.

Table 1: Initial conditions of the encounter and propagation. Earth and 2021 PDC* ephemeris retrieved at 2021 October 20 17:09:36 TDB, then tuned for an encounter with a circular planet. Pre-encounter elements correspond to the selected coordinates in the $\{k = 7, h = 5\}$ resonant circle: $\{\xi = -184, \zeta = -22,989\}$km

Body	$a(km)$	e	$i(deg)$	$\Omega(deg)$	$\omega(deg)$	$M_0(deg)$
Earth	147,003,315	0.016493	0.0042792	188.71	277.12	283.25
Earth circular ecliptic	147,003,315	0	0	188.71	277.12	283.25
2021 PDC*	135,862,510	0.40297	20.517	207.23	137.41	18.455
Pre-encounter	135,862,029	0.40293	20.517	207.26	137.40	17.509
Post-encounter	131,083,462	0.28747	20.832	207.26	121.00	33.876

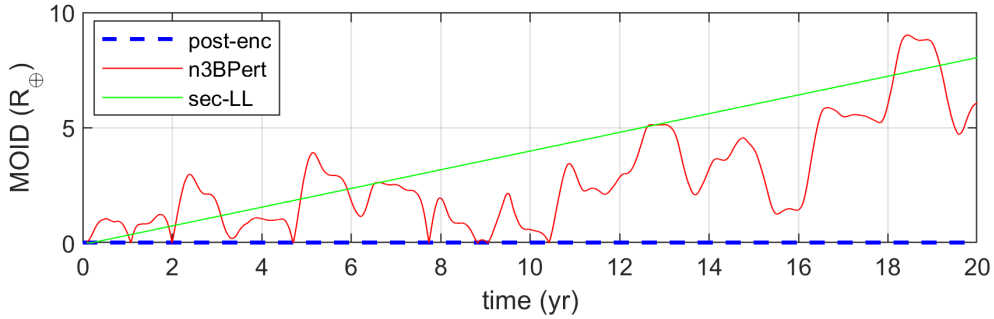

Figure 4: Earth MOID $(R_\oplus)$ of the fictitious 2021 PDC that crosses the resonant circle $\{k = 7, h = 5\}$ using three models: constant set of heliocentric elements (blue), secularly perturbed by Jupiter using the Lagrange-Laplace solution (green) and by numerical integration with the 8 planets as third-body perturbers (red). Time is measured in Earth periods from the 2021 encounter epoch with initial conditions as in table 1.

The propagated MOID defines whether a collision is possible at the time of the resonant encounter. Even if the point was initially selected in the keyhole region, the propagated MOID indicates that a collision is no longer possible in the corresponding resonant encounter. For this reason, in the following section the variation in the MOID is considered in the definition of the keyholes of flybys.

4. Modified Keyhole Computation

A keyhole is the locus of points on the B-plane leading to a collision after the next encounter; i.e., it is the pre-image of the Earth on the B-plane of the first encounter. In order to find keyholes multiple points along the resonant circles are tested. This section describes the conditions for a point to be a keyhole and how these are modified by a time-varying MOID.

If the heliocentric post-encounter Keplerian elements are assumed constant between encounters, the ξ coordinate that represents the MOID remains constant as well. However, using the MOID propagation methods we can model different perturbing effects and include them in the computation of keyholes. The points that fulfil the keyhole conditions accounting for the MOID variation are what we name modified keyholes. First, we detail the method of [2] for the computation of keyholes under unperturbed MOID. Then, we show the derived modification to obtain the new keyhole regions and the application to the flyby of 2021 PDC.

4.1. Constant elements between encounters

The coordinates that define a keyhole K are found as follows. The condition for a collision in the resonant encounter $(')$ is that the MOID ξ' is smaller or equal to the radius of collision b_p. Under the assumption that the MOID is unchanged by the Keplerian propagation $(\xi' = \xi)$, we can define the necessary condition for a given (ξ_K, ζ_K) to belong to a keyhole as:

$$\xi'_K = \xi_K = \xi'(U, \theta, \xi_K, \zeta_K) \leq b_P = R_P \sqrt{1 + \frac{2GM_P}{R_p U^2}} \tag{29}$$

where R_P and M_P are the planet's radius and mass, respectively. If the above condition is satisfied, a root-finding algorithm is used to find the value $\zeta_{K,0}$ that corresponds to a direct impact with Earth,

$$\zeta'_{K,0} = \zeta'(U, \theta, \xi_K, \zeta_{K,0}) = 0 \tag{30}$$

where the function ζ' is obtained from the solution of the encounter as described in section 2.3. Thus, using the approximation in ζ":

$$\zeta'' \approx \frac{\partial \zeta''}{\partial \zeta}|_{\zeta=\zeta_{K,0}} (\zeta - \zeta_{K,0}) \tag{31}$$

the upper and lower bounds of the keyhole are:

$$\zeta_{K,u} = \zeta_{K,0} + \frac{\sqrt{b_P^2 - \xi''^2_K}}{(\partial \zeta''/\partial \zeta)_{\zeta=\zeta_{K,0}}} \tag{32}$$

$$\zeta_{K,l} = \zeta_{K,0} - \frac{\sqrt{b_P^2 - \xi_K''^2}}{(\partial\zeta''/\partial\zeta)_{\zeta=\zeta_{K,0}}} \tag{33}$$

where the derivative $(\partial\zeta''/\partial\zeta)_{\zeta=\zeta_{K,0}}$ is

$$\frac{\partial\zeta''}{\partial\zeta} = hs(U',\theta')\frac{\partial\cos\theta'}{\partial\zeta} + \frac{\partial\zeta'}{\partial\zeta} \tag{34}$$

The expressions to find the factor $s(U',\theta')$ and $\frac{\partial\zeta'}{\partial\zeta}$ are reported in [2]. The keyhole is constructed by repeating this procedure for each (ξ_k,η_k) on k: h resonant circle.

4.2. Modified keyholes by propagation of the MOID

For the following analysis, the keyhole criterion on ξ is modified by including the time propagated variation $\Delta\xi$. The regions that fulfill the keyhole conditions, having considered the $\Delta\xi$, are the modified keyholes. We estimate $\Delta\xi$ computing the MOID both at the initial and subsequent encounter, such that:

$$\Delta MOID = \Delta\xi' = \xi'' - \xi' \tag{35}$$

We follow two different approaches to compute the MOID as presented in Section 3: a secular propagation and the numerical integration including n_p third-body perturbers. The criteria to determine if a given (ξ_K,η_K) is part of the keyhole is the same. The condition on ξ_K becomes:

$$\xi'' = \xi' + \Delta\xi \leq R_c = R_P\sqrt{1 + \frac{2GM_P}{R_pU^2}} \tag{36}$$

Along the resonant circle the post-encounter semi-major axis remains constant (See eq. 11). However, the rest of post-encounters elements, and thus the MOID at the next encounter, vary along the resonant circle. Figure 5 shows the variation $\Delta\xi$ along the resonant circle $\{k=7,h=3\}$. Among either model, the propagated $\Delta\xi$ is very different depending on the sign of ζ. Within the circle there are regions clearly distinguishable by having similar values of $\Delta\xi$. This observation could allow the reduction of the computational burden of propagating numerous trajectories in these regions of the resonant circle.

The short-period perturbations have a very important role in the propagation of the MOID, as described in section 3.4. We show this effect in Figure 4, where we observe the propagation in time for a single point of the resonant circle. Thus, implying that the difference the secular and numerical propagation of the MOID has a strong temporal component. However, within the same resonant encounter date and circle, it is possible to find a certain agreement between both theories. We further observe this in Figure 5, where two different resonant circles are shown. In the case of the $\{k=7,h=3\}$ circle, the two models show very different distributions of MOID variation at the subsequent encounter. However, in the case of $\{k=9,h=5\}$ the two distributions find a good level of agreement. This shows the potential of the analytical secular model to be used for preliminary analysis. However, this agreement need to be taken carefully since it depends on the flyby geometry and on the resonant circle. The use of a more complex analytical model can potentially reduce the differences with the numerical propagation. For example, the reconstruction of the short-period terms could significantly improve the accuracy of the analytical model.

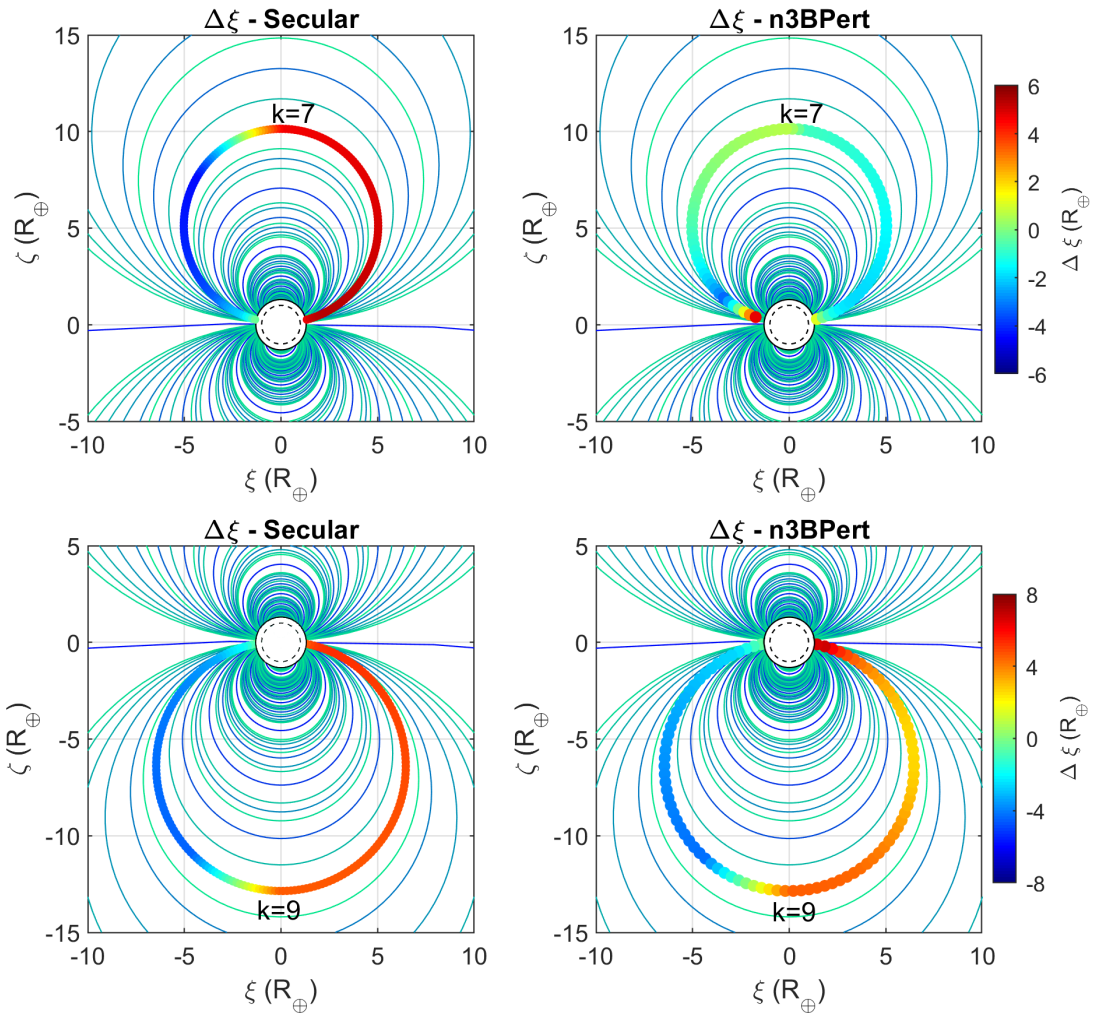

Figure 5: Variation of the MOID $(R_\oplus)$ at the resonant encounter around the resonant circles $\{k = 7, h = 3\}$ and $\{k = 9, h = 5\}$ using two models: secular propagation as perturbed by Jupiter using the Lagrange-Laplace solution (left) and by numerical integration with the 8 planets as third-body perturbers (right).

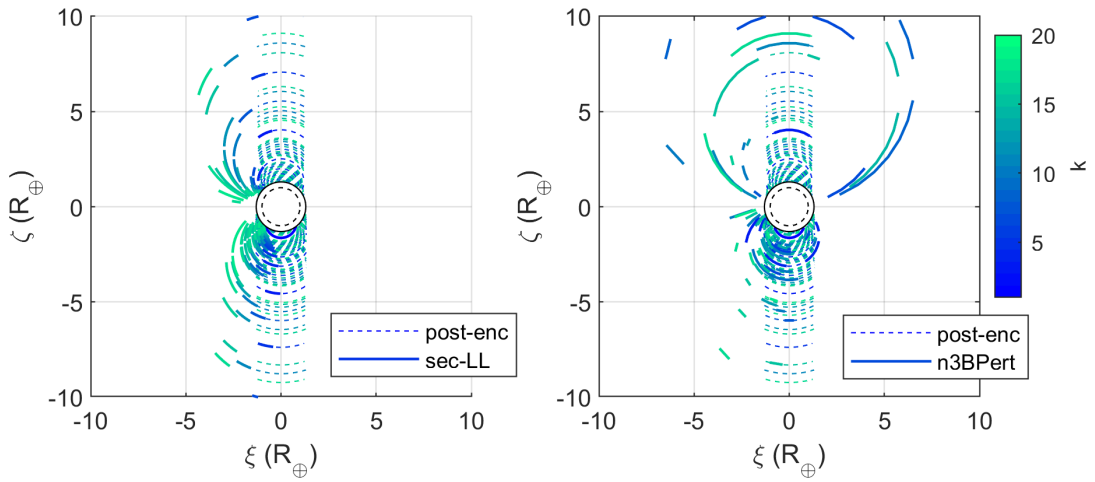

Figure 6: Modified keyholes of the Earth flyby of 2021 PDC for up to $k = 20$ Earth revolutions. Reference keyholes (dashed) obtained assuming constant elements, by secular propagation of the MOID (left, continuous) and numerical integration of the 8 planets as third-body perturbers (right, continuous).

The variation $\Delta\xi$ is computed in every point of the resonant circle to determine the modified keyholes. Figure 6 shows the modified keyholes of the 2021 PDC flyby computing the variation $\Delta\xi$ with the secular model and numerical integration. A large fraction of the keyholes that were obtained assuming constant heliocentric elements between encounters disappears or is translated to a different region of the B-plane. In general, the effect of the secular perturbation for this flyby is a displacement of the keyholes towards $-\xi$ that increases with k, the date of the resonant encounter. The short-period effects in the numerical propagation cause unpredicted $\Delta\xi$ variations. These variations translate into more disperse keyhole regions. In the third quadrant of the B-plane we observe similarities between both models, especially close to the $\xi = 0$ axis, with modified keyholes that can exist at higher ζ in resonant encounters further in the future.

5. 2021 PDC Flyby: Eccentric Earth

The computation of resonant encounters and keyholes is very sensitive to the initial conditions of the flyby. This natural sensitivity causes that modifications in the considered dynamics reflect into large differences in the analysis of the flyby. In this section we show the analysis of the 2021 flyby considering the eccentricity and inclination of Earth as retrieved at the ephemeris date in table 1[4]. With a time-varying distance to the central body, the ξ coordinate does not exactly match the MOID between planet and asteroid.

The first step of the resonant encounter analysis is the computation of the resonant circles. It is important to note that we approximate $\Delta\xi$ as the change in MOID although this is not strictly true when the eccentricity of the planet is considered. Figure 7 shows the new resonant circles when considering the eccentricity and inclination of Earth in the flyby. The main difference with the circular case in figure 2 is a larger asymmetry around $\zeta = 0$, with less circles in the $\zeta > 0$ half-plane. The computation of keyholes is heavily impacted by the different dynamics. In this specific flyby, the predicted keyhole regions stay within $3R_\oplus$ as described in figure 7.

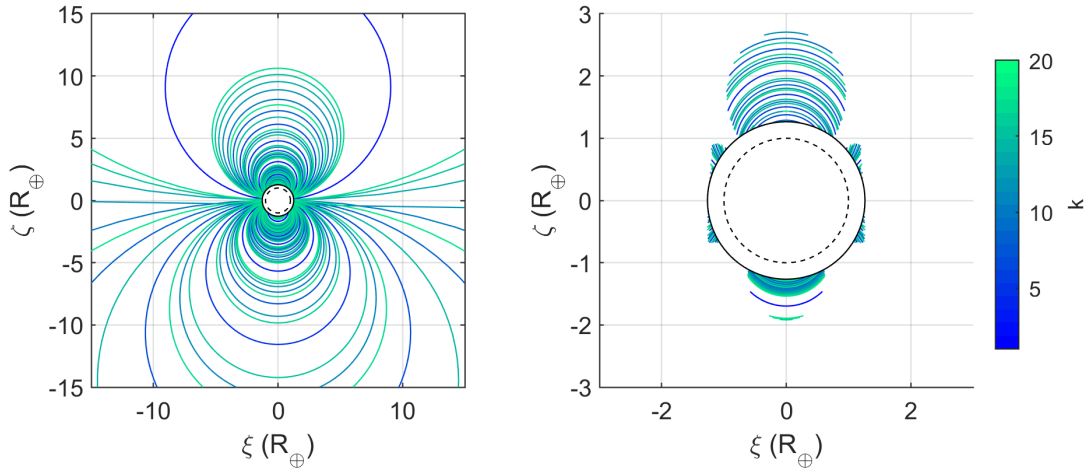

Figure 7: Resonant circles (left) and keyholes (right) of the Earth flyby of 2021 PDC for up to $k = 20$ Earth revolutions. The white circle represents the Earth radius with its gravitational focusing factor and the physical radius (dashed). The eccentricity in the orbit of the Earth is herein considered.

[4]Eccentricity and inclination of Earth are set to the osculating elements at the ephemeris retrieval epoch in the mean ecliptic and equinox frame of J2000. These elements are kept constant in the numerical integration of the perturbed MOID. In general, due to planetary perturbations, these are not constant.

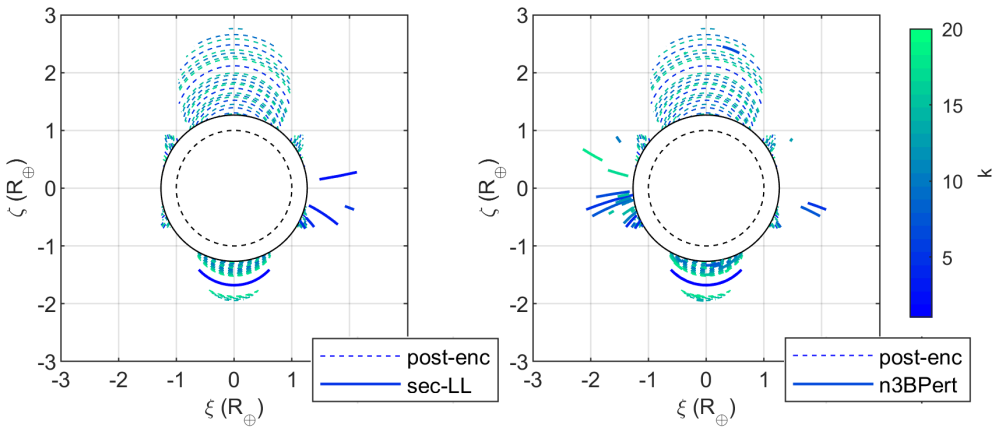

Figure 8: Modified keyholes of the Earth flyby of 2021 PDC for up to $k = 20$ Earth revolutions. Reference keyholes (dashed) obtained assuming constant elements, by secular propagation of the MOID (left, continuous) and numerical integration of the 8 planets as third-body perturbers(right, continuous). The eccentricity in the orbit of the Earth is herein considered.

Next, we can compute the modified keyholes using the same method used in the circular Earth orbit case (Fig.8). Similarly to the previous case, some modified keyholes appear in regions with higher pre-encounter $|\xi|$. This is because the variation $\Delta\xi$ contrasts the initially larger ξ. In the secular case, these appear for a few of the low k resonant circles in the $\xi > 0$ half-plane. The modified keyholes obtained through the numerical propagation of the MOID, slightly more numerous than in the secular case, appear mostly in the $\xi < 0$ sector. In general, further work is desired to better characterize this more generic case.

6. Conclusions

Our results show that the assumption of Keplerian motion between encounters has limitations in order to properly identify keyholes. By computing the expected variation in MOID, $\Delta\xi$, we were able to detect significant displacements of the keyholes, and to discard or consider new ones. Therefore, our results motivate the modelling of non-Keplerian effects in the heliocentric orbit of the asteroid in the preliminary analysis of keyholes.

The evolution of the MOID for 2021 PDC has a strong short-period component, with variations of a few Earth radii in months. The extension to consider the eccentricity of the Earth poses additional challenges. Future work includes improving the mapping from ΔMOID to $\Delta\xi$ as we move away from the circular assumption. Moreover, the effects of the non-zero inclination of the Earth should also be assessed.

On the other hand, in order to reduce the computational cost of the numerical approach, propagating only selected points in the resonant circles could help reduce the required time significantly. The presented approach is to uniformly distribute in space the points of the circle so that we can still capture regional behaviors. A direct application would be to make the selection based on the flyby uncertainty if available. In such case, the search for modified keyholes could be based on the intersections between the known line of variations and the resonant circles.

In conclusion, these results encourage the study of additional asteroids to explore the potential of finding modified keyholes without the use of large scale Monte Carlo simulations. We prove that the changes in $\Delta\xi$ can be significant and that an analytical secular model can partially capture the dynamics of the MOID. The proposed methodology leaves room to improve our dynamics models to ensure higher fidelity in the simulations. Along these lines, adding additional perturbations could be incorporated such as the Yarkovsky effect. Further, the accuracy of the secular model could be significantly improved by recovering short-periodic effects from the mean elements.

Acknowledgments

This research has made use of data and/or services provided by the International Astronomical Union's Minor Planet Center. This research is funded by the Balsells Fellowship Program at the University of Colorado Boulder and by a grant from the California Institute of Technology / Jet Propulsion Laboratory.

References

[1] D. Farnocchia, S. Eggl, P. W. Chodas, J. D. Giorgini, S. R. Chesley, Planetary encounter analysis on the B-plane: A comprehensive formulation, Celestial Mechanics and Dynamical Astronomy 131 (2019) 36.
[2] G. B. Valsecchi, A. Milani, G. F. Gronchi, S. R. Chesley, Resonant returns to close approaches: Analytical theory, Astronomy & Astrophysics 408 (2003) 1179–1196.
[3] G. B. Valsecchi, E. M. Alessi, A. Rossi, An analytical solution for the swing-by problem, Celestial Mechanics and Dynamical Astronomy 123 (2015) 151–166.
[4] J. Hernando-Ayuso, D. Amato, C. Bombardelli, Last-Minute Semi-Analytical Asteroid Deflection by Nuclear Explosion, p. 16.
[5] R. Greenberg, A. Carusi, G. Valsecchi, Outcomes of planetary close encounters: a systematic comparison of methodologies, Icarus 75 (1988) 1–29.
[6] G. Tommei, Algoritmi per il monitoraggio di possibili impatti asteroidali, Ph.D. thesis, Thesis, University of Pisa, Pisa, Italy, 2002.
[7] W. M. Folkner, J. G. Williams, D. H. Boggs, R. S. Park, P. Kuchynka, The Planetary and Lunar Ephemerides DE430 and DE431, Interplanet. Netw. Prog. Rep (2014).
[8] T. Wisniowski, H. Rickman, Fast geometric method for calculating accurate minimum orbit intersection distances, Acta Astronomica 63 (2013) 293–307.
[9] C. D. Murray, S. F. Dermott, Solar System Dynamics, Cambridge University Press, 2000.
[10] L. F. Shampine, M. W. Reichelt, The matlab ode suite, SIAM journal on scientific computing 18 (1997) 1–22.